Microchimica Acta (2024) 191:615
https://doi.org/10.1007/s00604-024-06672-y

ORIGINAL PAPER

Insights into solid-contact ion-selective electrodes based on laser-induced graphene: Key performance parameters for long-term and continuous measurements

Raquel R. A. Soares[1] · Gustavo L. Milião[1] · Cícero C. Pola[1,4] · Dapeng Jing[2] · Jemima Opare-Addo[3] · Emily Smith[3] · Jonathan C. Claussen[1] · Carmen L. Gomes[1]

Received: 1 June 2024 / Accepted: 26 August 2024 / Published online: 23 September 2024

Abstract

This work aims to serve as a comprehensive guide to properly characterize solid-contact ion-selective electrodes (SC-ISEs) for long-term use as they advance toward calibration-free sensors. The lack of well-defined SC-ISE performance criteria limits the ability to compare results and track progress in the field. Laser-induced graphene (LIG) is a rapid and scalable method that, by adjusting the CO_2 laser parameters, can create LIG substrates with tunable surface properties, including wettability, surface chemistry, and morphology. Herein, we fabricate laser-induced graphene (LIG) solid-contact electrodes using different laser settings and subsequently convert them into ion-selective sensors using a potassium-selective membrane. We measure the aforementioned tunable surface properties and correlate them with resultant low-frequency capacitance and water layer formation in an effort to pinpoint their effects on the sensitivity (Nernstian response), reproducibility (E°' variation), and potential stability of the LIG-based SC-ISEs. More specifically, we demonstrate that the surface wettability of the LIG substrate, which can be tuned by controlling the lasing parameters, can be modified to exhibit hydrophobic (contact angle > 90°) and even highly hydrophobic surfaces (contact angle ≈ 130°) to help reduce sensor drift. Recommendations are also provided to ensure proper and robust characterization of SC-ISEs for long-term and continuous measurements. Ultimately, we believe that a comprehensive understanding of the correlation between LIG tunable surface properties and SC-ISE performance can be used to improve the electrochemical behavior and stability of SC-ISEs designed with a wide range of materials beyond LIG.

Keywords Solid-contact ion-selective electrodes · Potential stability · Potentiometry · Graphene-based sensors · Laser scribing · Surface wettability

Background

In the following sections, we aim to provide useful information on properly characterizing solid-contact ion-selective electrodes (SC-ISEs) and their key performance parameters for long-term and continuous measurement applications. In particular, we provide an overview of the theoretical foundations of SC-ISEs and highlight the key figures of merit for SC-ISEs, providing a guiding reference on best practices for measuring and interpreting them. We present, through practical examples, SC-ISEs based on laser-induced graphene (LIG) with tunable surface properties, the correlation between solid-contact surface properties and SC-ISE performance using the recommended methods and discuss how the understanding of their effects can assist in improving potentiometric response and reduce potential drift.

✉ Jonathan C. Claussen
jcclauss@iastate.edu

✉ Carmen L. Gomes
carmen@iastate.edu

1 Department of Mechanical Engineering, Iowa State University, Ames, IA 50011, USA

2 Materials Analysis and Research Laboratory, Iowa State University, Ames, IA 50011, USA

3 Department of Chemistry, Iowa State University, Ames, IA 50011, USA

4 Department of Food Science and Human Nutrition, Iowa State University, Ames, IA 50011, USA

Sensitivity

In the context of ion-selective electrodes (ISEs), sensitivity refers to the ability of the electrode to detect and respond to changes in the activity of specific ions within the sample solution [1]. In other words, sensitivity can be defined as the ratio between variations in the output signal and the input variable, which are the electromotive force (EMF) and the ion activity, respectively. Ideally, potentiometric ISEs exhibit a Nernstian response when the system is in equilibrium, meaning that the measured potential (the output signal) is directly proportional to the logarithm of the ion activity (input variable), following the Nernst Equation (Eq. S1) [2]. See supplementary information (SI) for more details.

The sensitivity of ISEs directly influences the limit of detection (LOD), establishing an inverse relationship between these parameters. As sensitivity increases, the electrode can detect smaller changes in ion activity, leading to a lower LOD. According to the IUPAC traditional definition, the LOD for general analytical devices is typically calculated as three times the standard deviation of the blank readings divided by its sensitivity (Eq. S8) [3]. However, considering the logarithmic response of ISEs, their LOD is alternatively defined as the smallest concentration in which the potentiometric response (EMF) deviates significantly from the average EMF observed in the flat region of the calibration curve (Fig. 1) [4]. For practical convenience, the LOD value is determined as the intersection point obtained from the extrapolation of the two linear segments observed in an ISE calibration plot (Fig. 1) [5–7]. One of the linear segments corresponds to the Nernstian region and is determined by the slope of the calibration curve. The other linear segment originates from the baseline and the initial low concentrations of the target ion, which are difficult to differentiate from the blank due to unpredictable fluctuations of EMF. The reliability of the estimated LOD will depend on the experimental conditions, uncertainties associated with the calibration curve, and the significance level accepted [8]. For instance, the estimated baseline noise and the EMF variability in the Nernst region must be incorporated into the analysis for a probabilistic determination of the LOD. Hence, the minimum (LOD_{min}), the most probable (LOD_{mean}), and maximum (LOD_{max}) LOD values can be determined as the intersection points from the extrapolated linear segments and their confidence intervals (Fig. 1) [8].

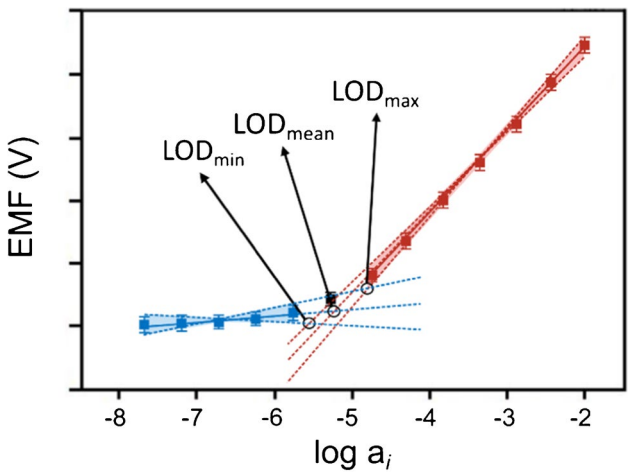

Fig. 1 The usual method for determining the limit of detection (LOD) for potentiometric ISEs

The sensitivity of ion-selective electrodes relies on several factors. One determinant is the composition of the ion-selective membrane (ISM), e.g., the type and quantity of ionophore, which impacts membrane quality [9, 10]. Higher ionophore concentrations can enhance selectivity and sensitivity, but there is a saturation point beyond which further addition does not yield improved results [11]. A well-established calibration curve with standard solutions within relevant concentration intervals is equally important to obtain and sustain sensitivity and accuracy. While there is no consensus on the extent acceptable of variation, a recent review by Rousseau and Bühlmann (2021) [12] describes, based on their own experience, that a deviation of up to 2 mV/decade falls within an acceptable margin of error for routine experiments. Additionally, membrane conditioning, which consists of immersing the ISE in a solution with the target ion for 24 h before measurements, contributes to better sensitivities within the desired concentration range [13, 14]. This conditioning also directly influences the LOD values [7].

***Note*:** Sensitivity (slope) values close to theoretical values do not guarantee a reliable performance of tested ISEs [12, 15]. Other aspects, such as reproducibility and stability, should be verified, as further discussed. On the other hand, if the calibration curve slope deviates from the Nernstian slope, it indicates an inadequate ISE.

Reproducibility

The main goal of sensor development is to provide accurate and reproducible devices that ideally do not require recalibration before usage (calibration-free) and exhibit high device-to-device reproducibility. This is particularly relevant for in-field devices and remote environmental sensors intended for long-term and continuous monitoring applications [16]. In the case of ISEs, reproducibility refers to the ability of the electrode to consistently yield similar EMF measurements when exposed to the same ion concentrations under the same conditions. Then, the definition of reproducibility is often expressed as the standard deviation of the formal potential (E°'), also represented by ΔE°', which considers the vertical shift (y-intercept) of the extrapolated

linear curve derived from the Nernstian behavior to 1 M of the primary ion, where log (1) = 0 (Fig. 2). Higher reproducibility is associated to lower ΔE°'. The estimation of this parameter can be derived from calibrations conducted on the same sensor, comparisons among multiple sensors within the same batch, or across various batches, depending on the purpose of the study. It serves as a critical metric for assessing the consistency and reliability of ISEs. As previously stated, the main criterion to identify if a potentiometric sensor can be considered calibration-free is the reproducibility of its E°' [15].

Considering that calibrations are performed under the same conditions, the slope and other pertinent variables (see SI for more details) should remain constant, attributing any shift on the y-axis primarily to changes in the intercept. The variations that cause this shift can originate from diverse factors known as "parallel processes," electrode aging, and operational errors. These parallel processes arise from variations in environmental parameters, such as temperature, pH, light, or dissolved gases [17]. Addressing reproducibility directly relates to the discussion of EMF drift, a topic further elaborated in subsequent sections, as it is a critical factor influencing the ΔE°'.

A common misconception concerning the reproducibility of ISEs is the assumption that repeated values for slopes (sensitivity values) obtained from calibration curves suggest highly reproducible electrodes [15]. This statement contradicts the previously mentioned concept, as it overlooks the ΔE°', a key parameter in assessing reproducibility. There is no consensus regarding the acceptable range of deviations for E°'. A recent review by Rousseau and Bühlmann (2021) [12] describes ΔE°' ranging from ± 0.1 to 10 mV depending on the ISE composition (ionophore, membrane composition, and electron-conducting substrate). The E°' can vary from changes in the phase boundary potentials at any of the interfaces in the electrochemical cell [12]. For achieving calibration-free ISEs, a standard deviation lower than 1 mV would be acceptable [18]. To reliably estimate the ion activity by measuring the EMF, reducing the ΔE°' is imperative, which means improving reproducibility. This action requires robust calibrations. Additionally, regular verification of electrode calibration is an important quality control for maintaining reproducibility. Hence, reporting the ΔE°' as a comparative parameter remains essential for assessing how reproducible a sensor can be.

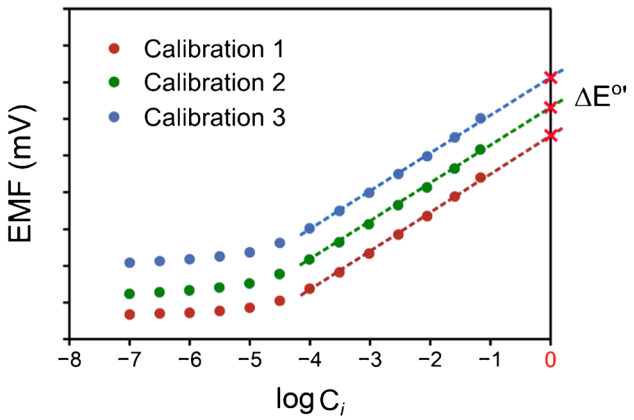

Fig. 2 Schematic visualization depicting vertical shifts (y-intercept) among calibration curves, resulting in a large ΔE°'. The hypothetical blue, green, and red calibration curves represent measurements taken on the same sensor but exhibit different y-axis intercepts. Note: Calculate ΔE°' as the standard deviation of all intercepts when comparing multiple calibrations

***Note*:** While the ΔE°' is the most critical parameter to consider for a calibration-free SC-ISE sensor, the slope of the calibration curve is also important [15]. If the sensor is operating correctly, the variation from the theoretical Nernstian slope should be minimal, and the standard deviation of the slope obtained experimentally should be small (see the "Potential stability" section). Another critical factor is the potential stability of reference electrodes, as any potential drift is the result of the drift contributions from the ISE and the reference electrode. Many commercial reference electrodes showed increased drifts compared to highly optimized SC-ISEs without proper use [10]. To verify reference electrode potential stability and other considerations for experiment set-up and reporting, refer to Rousseau and Bühlmann (2021) [12].

Potential stability

In potentiometric sensing, "drift" refers to a gradual change in measured potential over time. The duration and magnitude of this change determine the necessity for sensor recalibration, with established standards to ensure accuracy and reliability. Solid-contact ion-selective electrodes (SC-ISEs) represent the most widely used potentiometric sensors [19]. Current efforts focus on achieving calibration-free ISEs, minimizing drift to such an extent that recalibration becomes unnecessary [20]. Due to the logarithmic relationship between activity and EMF, a variation of ± 1 mV in EMF results in increasing variation in activity, particularly noticeable as the measured potential increases in magnitude. The 1-mV variation consistently introduces a constant error percentage of 4% (0.0396) for monovalent ions regardless of the EMF [15], as illustrated in Fig. 3. Similarly, a 2-mV change in the measured potential would result in an error of 8%, a 3-mV change would correspond to a 12% error, and so forth. The percentage error increases twofold for divalent ions. The significance of the drift depends on the acceptable range established by the application or the acceptable margin of error. For instance, variations of 4 mV/h would provide a ± 16% error in terms of accuracy for detecting a monovalent ion [21]. In scenarios where recalibrations are

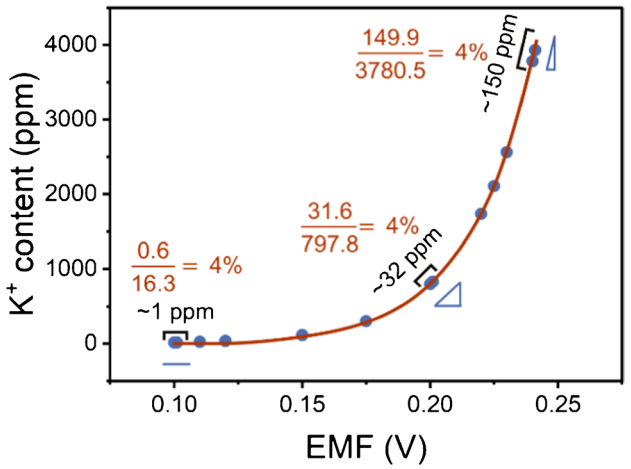

Fig. 3 Variations of 1 mV are depicted for a representative example of a monovalent ISE using a generic equation $y = 59.2\ \log(x) + 0.3$. While a 1 mV change results in less than 1 ppm variation for lower EMF values, this ratio consistently yields a 4% error, even with larger activity variations observed at higher EMF values

doable, the tolerance for variations in EMF can vary widely, dictated by specific application requirements. Recalibration of ISEs through a one-point method and the correction of the initial calibration curve are commonly performed for ISEs used in medium- or long-term measurements (hours to days) [22]; consequently, the frequency of recalibration becomes important.

To discuss potential drift or stability without mentioning ΔE°' is challenging, as they are inherently linked in a cause-and-effect relationship. When a sensor exhibits large EMF fluctuations over time, it will generate shifted calibration curves, which, in turn, will generate a substantial ΔE°'. Potential drift is often associated with a state of non-equilibrium between the sample and the sensing membrane, as reviewed previously [12]. This non-equilibrium state may arise from various factors, including ion complexation equilibrium within the sensing membrane, ion fluxes resulting from sensor exposure to elevated concentrations of interfering ions before acquiring measurements in the primary ion solution, non-linear responses within the tested activity range at the lower or upper LOD, and susceptibility to polarization at interfaces [16]. These contributing factors to potential drift highlight the importance of a stable output signal as a prerequisite for reliable measurements.

A common approach to assessing the potential stability of ISEs involves reporting the low-frequency capacitance (C_L), which is acquired through chronopotentiometry at a small applied current [23]. A higher capacitance often correlates with improved potential stability or reduced potential drift. Understanding and optimizing the low-frequency capacitance profile contributes to developing more stable and reliable potentiometric sensors and is a key performance parameter for comparing different SC-ISE materials. The low-frequency capacitance can be increased by increasing the solid-contact surface area and, consequently, the interfacial area between the solid contact and the sensing membrane. It can be achieved through various techniques that increase surface roughness, such as physical or chemical etching and laser etching. Das et al. (2016) [24] showed a scalable method for creating 3D graphene petals using inkjet-printed followed by a laser processing. This technique significantly enhances the surface area by transforming a 2D printed graphene surface into a high-surface area 3D morphology. Consequently, ISEs utilizing high-aspect ratio materials as solid contacts have demonstrated remarkable potential stability [10, 16].

The methodology employed to determine the low-frequency capacitance in ISEs involves the application of a small constant current sufficient to polarize the electrode within the range of nanoamperes (nA) to picoamperes (pA) [25]. Typically, an electrode is polarized by applying ± 1 nA for 60 s each while recording the resulting potential response (mV) [23]. This technique allows for observing potential drifts induced by the low current while measuring the electrode's capacitance. The behavior of the electrode at low current resembles an RC (resistor–capacitor) equivalent circuit [16]. In ideal circumstances with perfectly stable ISEs, we expect to observe a constant EMF unaffected by the small applied current, as illustrated in Fig. 4a. However, in practical scenarios, all solid contact ISEs can be polarized to some level. The higher the electrode capacitance, the smaller the potential drift, as shown in Eq. S9. The capacitance values obtained from this equation correlate well with those obtained by electrochemical impedance spectroscopy (EIS) measurements [26]. Assuming a maximum potential drift of 1 mV/h, as expected for long-term measurement, and after measuring the current of 1 pA, based on Eq. S9, a minimal electrode capacitance of 3.6 µF is needed [16].

***Note*:** Using chronopotentiometry to obtain low-frequency capacitance is an approach for estimating short-term potential drift through experiments lasting only a few minutes. Measuring low-frequency capacitance in a solvent that thoroughly wets the ISE, with the corresponding electrolyte and reference electrode, is also recommended to fully understand the electrode's capacitive behavior [18, 26, 27]. Whenever possible, it is recommended to report specific capacitance values (F/g) by dividing the measured capacitance by the mass of the solid-contact material, allowing for comparison among studies [10]. While C_L values provide valuable information on the solid-contact/ISM interface interactions, other methods should be considered regarding long-term drift, which measures the potential over extended periods (multiple hours to days) while the electrode is immersed in a solution of known ion concentration [10].

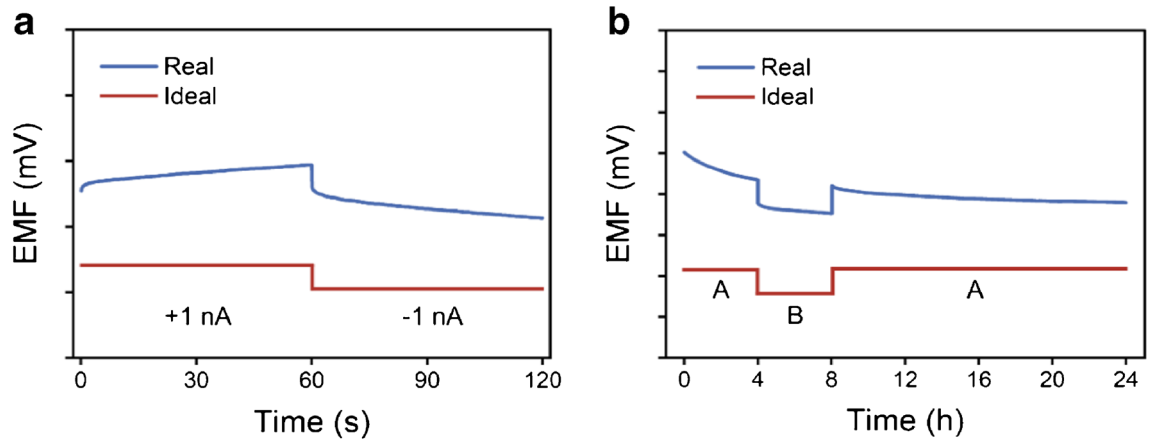

Fig. 4 **a** Schematic illustration showing results of chronopotentiometric test for an ideal (red) and a typical (blue) SC-ISE. A current of ± 1 nA for 60 s each is applied to the ISE while the EMF is measured. **b** A visual representation of a 24-h water layer test involving sequential solution conditioning (A: primary ion, B: interfering ion) for a typical (blue) with ideal (red) SC-ISEs. Note: The observed reduction in potential (EMF) in **a** upon switching from + 1 nA to -1 nA is the Ohmic drop (*2 i R*, where *R* is the cell resistance). This phenomenon reflects the decrease in potential due to the inherent resistance of electrolyte and electrode materials [16]

Another key criterion for assessing potential stability is through a water layer test [23], which involves measuring potential drift over an extended period, often 24 h, while the electrode is sequentially conditioned in concentrated solutions of primary and interfering ions, as illustrated in Fig. 4b. This evaluation is typically achieved by measuring the EMF and reporting the potential drift over time as millivolts per hour (mV/h), providing insights into the formation of an aqueous layer between the selective membrane and the solid-contact material [6]. Potential drifts are observed at different test stages when this water layer is present. Notably, the potential differs from the original value (drift) when switching ion solutions between the primary to interfering ions, as shown in Fig. 4b (blue line). This phenomenon was first observed in 2000 when researchers noted potential drifts in SC-ISEs attributed to zero-current ion fluxes through the selective membrane [28]. When a water layer forms, the ISMs no longer function as true solid-contact ISEs, as a thin inner water layer develops between the solid-contact and the ISM [12]. This test is susceptible to ionic changes and functions as a reservoir for transmembrane ions and neutral species [23]. The thinner the water layer, the more sensitive it is to ionic changes. Consequently, the electrode is no longer selective to the primary ion, and the ion-to-electron transducer is considered to have partly failed. As the water layer expands across the electrode interface, the ISM will gradually delaminate from the solid-contact material, leading to mechanical failure [12, 23].

Lindner and Gyurcsányi (2009) [15] comprehensively reviewed the water layer test, emphasizing the importance of electrode preconditioning time, experimental equilibration time, and selection of appropriate interfering ions that can produce sufficient ion-exchange-induced fluxes across the membrane. These authors emphasized that electrodes that have ISM with low water diffusion coefficients should be evaluated over longer periods, and highly discriminated ions are not adequate for the test since they do not sufficiently enter the ISM to the extent needed to induce ion exchange. As previously reviewed, typical values for EMF drift usually fall within tens of µV/h or even mV/h [10, 12].

One approach to mitigate the formation of a detrimental water layer is to fabricate the ISM using a polymer with a reduced water diffusion coefficient, such as poly(acrylate) or polyurethane, compared to PVC and silicone rubber-based membranes. However, as noted by Hu et al. (2016)[16] and Shao et al. (2020) [23], all ISM polymers are susceptible to water uptake to an extent; therefore, an undesirable water layer can still be formed without considering the solid-contact properties. In hydrophilic materials, this layer tends to accumulate in the defect areas and edges between the ISM and solid-contact surfaces. In contrast, surfaces treated with fluorinated groups form a hydrophobic surface [29], for example, mitigating water layer formation. The addition of a fluorinated acrylic copolymer to colloid-imprinted mesoporous (CIM) solid contact material enhanced the surface hydrophobicity and further hindered the water layer formation, resulting in one of the lowest long-term drift of less than 1 µV/h over 50 h for a potassium-ISE reported so far [30]. Consequently, a hydrophobic solid-contact surface with enhanced adhesion of the ISM is essential to inhibit the water layer formation, which is discussed in the next section.

***Note*:** Drifts observed in the calibration curves, either from changes in the slope or shifts of the intercept (ΔE°'), or both, can be an indicator of water layer formation. Thus, these drifts should be monitored for long-term stability along with the traditional water layer test. As emphasized

by Chipangura et al. (2023) [10], these tests are more valuable when performed after long-term measurements.

Surface properties

Considering that ISMs are typically composed of a hydrophobic polymer, often with a plasticizer and other highly hydrophobic components [31], ensuring a hydrophobic solid-contact surface is one approach to prevent the formation of an aqueous layer at the interface of the solid-contact transducing layer and the ISM, thus mitigating potential drift [14, 32]. Static and dynamic contact angle measurements are used to determine wetting, dewetting, and adhesion characteristics of surfaces using a goniometer [33, 34] (See SI for more details). A surface is considered hydrophobic when its static contact angle θ is > 90°, hydrophilic when θ is < 90°, superhydrophobic when θ is > 145°, and superhydrophilic when θ equals 0° [33]. The wettability of the solid-contact surface can be evaluated using different solvents (a selection of polar and non-polar solvents). The adhesion between hydrophobic polymeric ISMs and solid contact surfaces benefits from a large surface area and penetration into the porous material within the solid-contact layer, as observed with nanostructured carbon materials [10]. Additionally, nanostructured carbon materials with high surface areas that have large pore sizes, which are accessible to ion-ionophore complexes, ionic sites, and other ISM components, have shown improved ISE performance (i.e., increased low-frequency capacitance and reduced drift), as reviewed by Chipangura et al. (2023) [10].

The wettability of a solid surface is highly affected by the physical structure (micro and nano-structuring) and surface chemistry (e.g., the presence of oxygenated groups for hydrophilic materials or fluorinated groups for hydrophobic materials) [35]. Typically, the wetting of a liquid on structured surfaces displays one of the two conditions: 1) the Wenzel wetting state, where water is in complete contact with the structure surface [36], or 2) the Cassie-Baxter wetting state, where water is in contact with the peaks of the structured surface and air pockets are trapped in between (e.g., lotus leaf, rose petals) [37].

Drift in potentiometric sensing is influenced not only by solid contact properties but also by ISM composition, contaminants on electrode surfaces, membrane degradation (e.g., via water layer formation), side reactions with light, redox couples, O_2 and CO_2, fluctuations in temperature, and issues related to reference electrode stability [23]. Consequently, comparisons among SC-ISEs are most relevant among systems using similar or identical ISM compositions when evaluating solid-contact properties. Thus, in this study, we selected a PVC-based system, the most commonly used ISM, with valinomycin as a potassium ionophore. To investigate the relationship between solid-contact surface properties and resulting electrochemical properties, we used laser-induced graphene (LIG) electrodes, a rapid and scalable method for electrode substrate production [14]. The CO_2 laser parameters are modified to create LIG with different electrical conductivity, surface morphology, and wettability with large surface areas that are then used as capacitive transducers in SC-ISEs. We demonstrate that SC-ISE potential stability can be improved, and water layer formation can be reduced with hydrophobicity tuning. We measure and correlate the corresponding surface properties with potentiometric sensing performance, including sensitivity, reproducibility, and potential stability.

Experimental section

Materials

Valinomycin (potassium ionophore I), potassium tetrakis(4-chlorophenyl)borate, poly(vinyl chloride) high molecular weight (PVC), bis(2-ethylhexyl) sebacate (DOS), tetrahydrofuran (THF), potassium hexafluorophosphate (KPF_6), and dimethyl sulfoxide (DMSO) were purchased from Millipore Sigma (Saint Louis, MO, USA). Commercial polyimide (PI) with 0.127 mm thickness was purchased from McMaster-Carr (Elmhurst, IL, USA), and silver-chloride epoxy ink (Cl-1001) from Engineering Materials Systems (Delaware, OH, USA). Acetonitrile, methanol, formamide, glycerol, potassium chloride, and sodium chloride were obtained from Fisher Scientific (Waltham, MA, USA). Castor oil was purchased from Heritage Store (Virginia Beach, VA, USA). Fast-drying nitrocellulose-based lacquer was obtained from L.A. Colors (Ontario, CA, USA), and the liquid electrical tape was purchased from Star Brite, Inc. (Montgomery, AL, USA). All solutions were prepared using deionized (DI) water with a resistivity of approximately 18.2 MΩ.cm.

Apparatus and techniques

Constant current chronopotentiometry (CP) measurements and calibration curves at open circuit potential (OCP) were performed using a CH Instruments electrochemical analyzer (model CHI7091E, CH Instruments Inc., Austin, TX, USA, input impedance 10^{12} Ω). Water layer tests were performed simultaneously with three sensors using a PalmSens4 potentiostat (PalmSens, Utrecht, Netherlands, input impedance 10 TΩ) equipped with a MUX8-R2 multiplexer. The electrodes were first exposed to 10 mM KCl for 4 h, followed by 10 mM NaCl for another 4 h, and finally returned to the initial target ion solution for a 16-h incubation step. Long-term stability was evaluated in 10 mM KCl for 72 h while monitoring the EMF signal. All experiments were conducted in a two-electrode cell with the potassium ion-selective electrodes as

the working electrode and an external Ag/AgCl electrode with a 1 M KCl liquid junction and a porous Teflon tip as the reference electrode (CH Instruments Inc., Austin, TX, USA). The CP measurements were performed in two different electrolyte solutions, 0.1 M KCl in DI water and 0.1 M KPF_6 in acetonitrile, after a 24-h conditioning step in these solutions. A current of ± 1 nA was applied for 60 s each (120 s total) while the EMF signal was recorded. Calibrations were performed from 10^{-7} to 10^{-1} M KCl, with additions at each 0.5 log, in DI water under agitation at 300 rpm. The results were presented as average ± standard deviation of measurements with four electrodes.

Top-view scanning electron microscopy (SEM) images of the fabricated LIG materials were acquired using a FEI Quanta 250 field emission microscope (FEI Technologies, Hillsboro, OR, USA). The images were captured at magnifications of 150×, 1500×, and 15,000×, with an accelerating voltage set at 10 kV. Before imaging, the samples were coated with a 2-nm iridium layer to enhance conductivity.

X-ray photoelectron spectroscopy (XPS) analysis was obtained using Kratos Amicus/ESCA 3400 (Kratos Analytical, Manchester, UK). The samples were irradiated with unmonochromated Mg K_α X-rays at 240 W, and the energy of vertically emitted photoelectrons was analyzed using a DuPont-type analyzer. The pass energy was configured to 150 eV, and the raw data was processed using CasaXPS (Casa Software Ltd., Teignmouth, UK).

The static contact angle measurements were obtained using a ramé-hart model 90 goniometer (ramé-hart instrument Co., Succasunna, NJ) with an automatic dispensing system using a 3-µL droplet of each solvent [14]. DROPimage Pro software generated and analyzed the images to determine the contact angles. The wettability of the three different fabricated LIG materials was evaluated using DI water, formamide, DMSO, glycerol, methanol, and castor oil.

Raman spectroscopy measurements were performed using a Horiba XploRA Plus confocal Raman microscope with a 532 nm laser operating at 1.2 mW and a 50× (0.5 numerical aperture) objective. The spectra were collected from 600 to 3000 cm^{-1} with a 600 grooves mm^{-1} grating. Ten Raman spectra were collected at ten randomly selected locations of the sample, and each spectrum was collected using a 30 s acquisition time and three accumulations. All Raman peaks in each spectrum were fitted to a Lorentzian function in Igor Pro 6.37. The I_D/I_G and I_{2D}/I_G ratios were calculated from the fitting results.

Fabrication of laser-induced graphene-based electrodes

The LIG-based electrodes were fabricated using a 75 W M2 Epilog CO_2 laser, operating at a wavelength of 10.6 µm (Epilog Laser, CO, USA) and 1200 dpi, directly applied onto a polyimide film under ambient conditions. Three distinct LIG surfaces were produced by varying fabrication settings. A superhydrophilic LIG was achieved at 15% speed and 7% power following a single lasing step. To obtain a hydrophobic LIG, an additional lasing step was applied to the initial settings at 20% speed and 3% power [14]. The resulting material from these dual lasing steps was stored at ambient conditions (23 ± 1 °C) for at least 1 week to obtain highly hydrophobic LIG. All fabrication procedures were maintained at a + 1 mm offset from the laser focal point.

The working electrodes, depicted in Fig. 5, were designed in a dipstick format featuring a circular working area of 5 mm in diameter. A square contact pad on the top was shielded with conductive silver paste. The intermediate section between these ends was isolated by applying a passivation layer using fast-drying nitrocellulose-based lacquer or electrical liquid tape when the electrodes were tested in water or acetonitrile, respectively.

The potassium-selective membrane was created by dissolving the compounds (1.06 wt.% valinomycin, 0.34 wt.% potassium tetrakis 4-chlorophenyl borate as the ionic site, 32.90 wt.% PVC, 65.70 wt.% DOS) in 1 mL of THF, as previously reported [38]. The mixture was vigorously stirred until complete dissolution. Subsequently, two aliquots of 10 µL of the prepared membrane were applied onto the working area of LIG-electrodes. After an overnight drying period, the ion-selective electrodes (ISEs) underwent 24-h conditioning in a 1 mM KCl solution before testing.

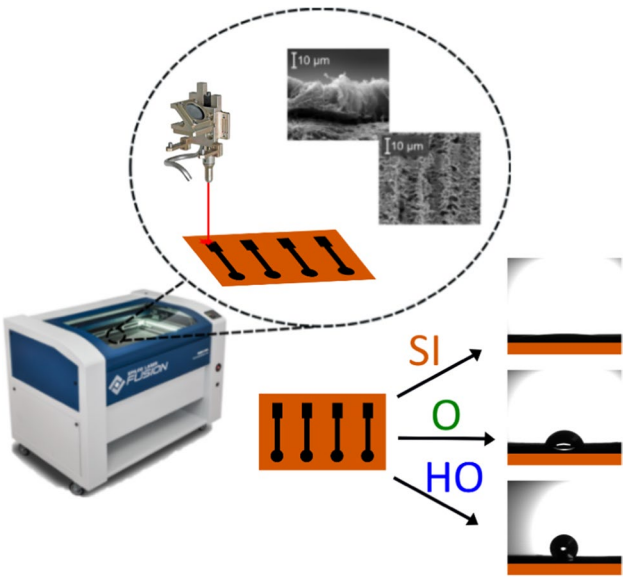

Fig. 5 Schematic illustrating the fabrication process of three distinct LIG materials: one lasing step resulting in a superhydrophilic surface (SI), two lasing steps for a hydrophobic surface (O), and two lasing steps combined with subsequent ambient storage resulting in a highly hydrophobic surface (HO)

Data analysis

Independent experiments in a completely randomized design were performed at least in triplicate and expressed as mean ± standard deviation. Analysis of variance (ANOVA) was used to test for significance, and the Tukey Honestly Significant Difference (HSD) test was used to separate the means at the significance level of 5% ($\alpha = 0.05$). Regression analysis with a confidence level of 95% was performed to determine the linear sensing range and the functional correspondence between ion activity and EMF. JMP Pro v.17 statistical software (SAS Institute, Cary, NC, USA) was used for the statistical analysis. Figures-of-merit were calculated using MATLAB (R2022a, The MathWorks Inc., Natick, MA, USA). All figures were plotted using OriginLab 2022b (OriginLab Co., Northampton, MA, USA).

Results and discussion

Surface properties

The effect of different laser settings and storage conditions on static contact angles (θ) for fabricated LIG with different standard liquids is shown in Fig. 6. Considering that one approach to suppress water layer formation between the solid-contact interface and the ISM is to have a sufficiently hydrophobic solid-contact surface (contact angle > 90° for water) [32], a rapid and scalable method to produce hydrophobic solid-contact materials is beneficial. The double-lasing process with and without ambient storage significantly reduced surface wetting (reduced the static contact angles) for DI water (surface tension, γ, of 72.75 mN m^{-1} [39]), with contact angles of 135.5° ± 4.5° and 95.3° ± 3.3°, respectively, while displaying θ ~ 0° for standard liquids with low surface tensions (e.g., θ = 0.0° ± 0.0° for both materials tested with methanol, $\gamma = 22.95$ mN m^{-1} [39]), demonstrating a decrease in the strength of interfacial forces with the double-lasing process and ambient storage, which hinders wetting by DI water (as recorded). Thus, these surfaces are hydrophobic and highly hydrophobic (θ > 90°), viz, O-LIG and HO-LIG. These static contact angles for DI water are similar to previously reported hydrophobic and highly hydrophobic LIG surfaces fabricated using the double-lasing process [14, 35, 40]. The increase in hydrophobicity of surfaces of graphene and graphite upon exposure to air has been associated with the surface adsorption of airborne hydrocarbons by Li et al. [41] and Hurst et al. [42] and, more recently, by Behrent et al. [43] for surfaces of LIG-based materials. Behrent et al. [43] noted that given the 3D-porous structure of LIG-based materials, the adsorption equilibrium of hydrocarbons to the surface occurs over a longer timescale (days to weeks) compared to graphite and graphene electrodes (minutes and hours).

Conversely, the single-lasing settings displayed a LIG surface with static contact angles ~ 0° for all standard liquids, with a slight increase observed for castor oil, indicating an increase in the strength of interfacial forces compared to the other LIG surfaces, which thus promotes wetting (as observed) [44]. The static contact angle for DI water was 0°, consequently, a superhydrophilic surface, viz. SI-LIG, while also exhibiting superoleophilic wetting properties with contact angles close to zero for standard liquids with low surface tension as shown in Fig. 6a (e.g., θ = 0.0° ± 0.0° for methanol, $\gamma = 22.95$ mN m^{-1}).

The wettability of a surface is closely related to its physical structure (i.e., micro and nano-structuring) and surface chemistry [35]. Notably, as depicted in Fig. 7, SI-LIG presents a 3D flaky network structure that seems to promote water absorption [45, 46]. Additionally, the double laser processing used to fabricate O-LIG and HO-LIG removes these flakes and promotes the formation of a porous matrix, resulting in a denser microporous structure [35]. The micro- and nano-structuring observed by the different laser processing under ambient conditions agree with previous studies [14, 35, 40]. This structural change enhances the incorporation of

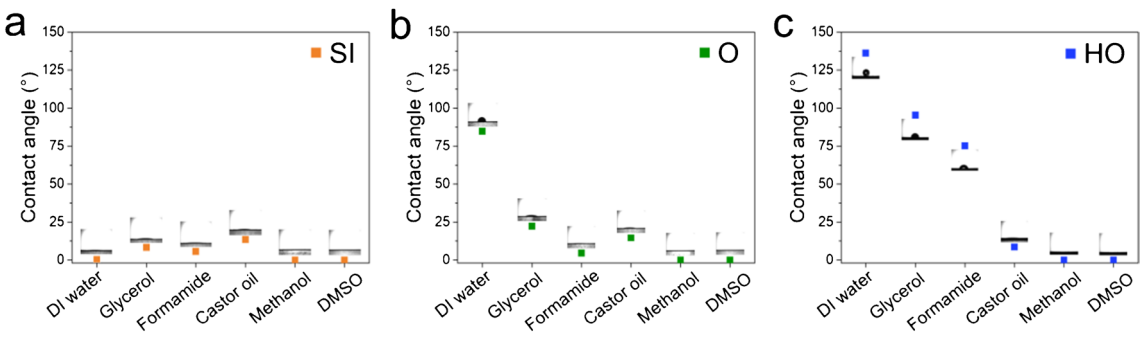

Fig. 6 **a–c** Static contact angle measurements and corresponding images of solvent droplets (DI water, glycerol, formamide, castor oil, methanol, and DMSO) for the three distinct LIG materials (SI-LIG, O-LIG, and HO-LIG)

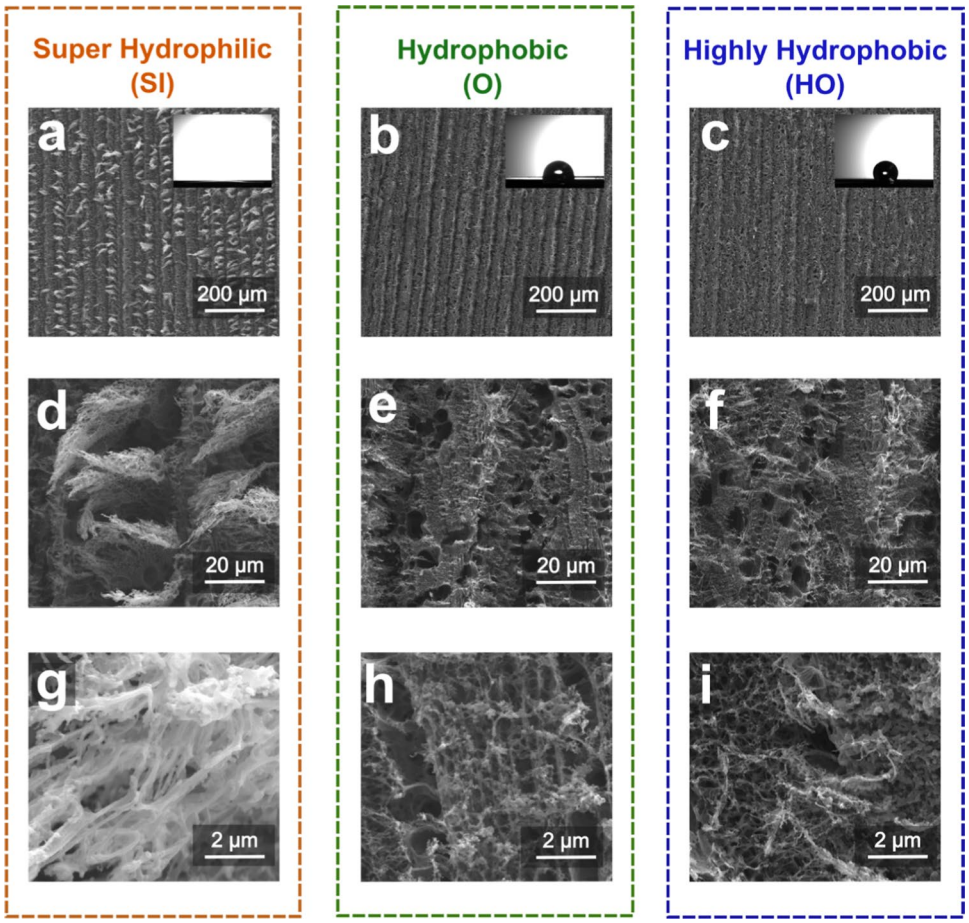

Fig. 7 SEM images at increasing magnifications (150×, 1500×, and 15,000×) and static contact angle photograph for DI water. **a-d-g** SI-LIG shows a flake-like structure. **b-e–h** O-LIG displays its porous characteristic with less flakiness compared to SI. **c-f-i** SO-LIG exhibits similar patterns as O but considerably higher hydrophobicity

air pockets trapped on the surface, consequently increasing the liquid–air interfacial area and promoting lower droplet adhesion to the LIG surface, characteristic of the Cassie-Baxter wetting state [35, 37].

The meso- and macro-porosity observed is not easily blocked by sub-nanometer scale surface oxides, which have been associated with physical adsorption suppression [44]. Therefore, surface chemistry plays a significant role along with surface micro and nano-structuring to surface wettability properties. The XPS analyses (see Fig. 8 and Table S1) showed that SI-LIG had a higher oxygen content (10.25 ± 0.70%) compared to the O-LIG (7.66 ± 0.92%), demonstrating that a higher oxygen content (via C-O, C = O, and O-C = O bonds) enhances the polar contribution to LIG surface energy, so that more O content means the surface edges are more favorable to interact with water, and thus

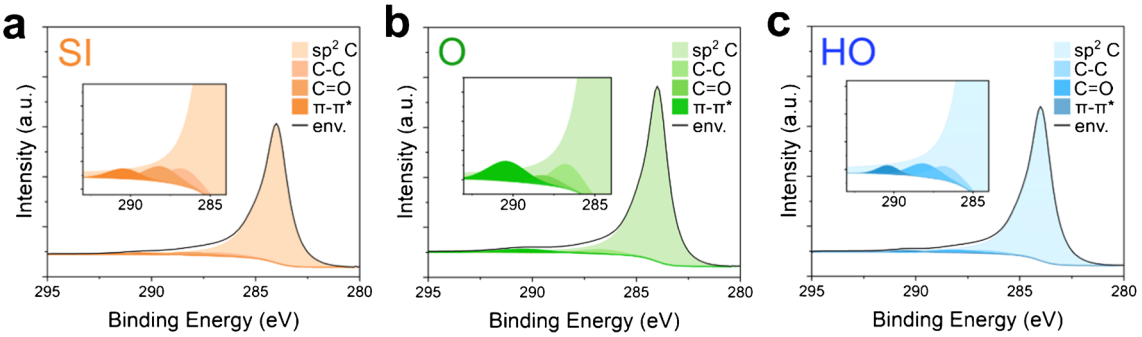

Fig. 8 High-resolution C1s XPS spectra of the three LIG materials. **a** SI-LIG. **b** O-LIG. **c** HO-LIG. The three plots are reported on the same scale

more hydrophilic [47]. However, the oxygen content does not explain the oleophilic behavior of SI-LIG. Furthermore, HO-LIG, stored under ambient conditions (23 ± 1 °C) for a minimum of 1 week, exhibited the highest oxygen content (11.78 ± 2.16%) among its counterparts, yet this difference was not statistically significant compared to SI-LIG ($p = 0.387$). This result leads us to hypothesize that prolonged exposure to air may have resulted in the adsorption of O_2 within the microporous structure of HO-LIG, thereby increasing the oxygen content in the material [48]. One should note that near-surface oxygen concentration obtained by XPS analysis is limited by the sampling depth, which is about 8 nm under the experimental conditions, as emphasized by Chen et al. (2003) [44]. Consequently, it can only capture as many as ~ 23 subsurface carbon layers (8 nm divided by 0.34 nm, thickness of single carbon atom layer) along with the oxygen-rich surface, which is insufficient to fully characterize the wettability and adsorption properties of porous LIG material. This observation raises the question of whether micro and nano-structuring may play a more significant role than surface chemistry in determining surface wettability properties, underscoring the need for further investigations. A detailed characterization of surface energy, their magnitudes, and the ratio of polar to dispersive energies is granted to further elucidate the LIG wetting properties. Next, the three LIG surfaces are converted to potassium ISE, and their corresponding electrochemical responses are evaluated.

The Raman spectra for all three materials showed the characteristic D, G, and 2D peaks typically found in LIG generated via CO_2-laser irradiation (Fig. 9) [49]. The D peak is associated with structural defects or misalignments in the three-dimensional structure of LIG [50]. The G peak corresponds to the in-plane vibrations of carbon atoms in sp^2 hybridization, while the 2D peak provides information about the stacking arrangement of graphene sheets [51]. The Raman spectra corroborated the XPS results regarding the amount of sp^2 carbon. The O-LIG and HO-LIG samples showed sharper 2D peaks compared to the SI-LIG sample (Fig. 9b), with the I_{2D}/I_G ratio for HO-LIG being significantly different from that of SI-LIG ($p = 0.090$). The XPS analysis also exhibited higher sp^2 carbon content for the O-LIG and HO-LIG materials (Fig. 8). Specifically, the I_{2D}/I_G ratios for SI-LIG, O-LIG, and HO-LIG were 0.53 ± 0.08, 0.59 ± 0.05, and 0.64 ± 0.08, respectively, suggesting that the formed graphene exhibits a multilayered structure, also referred to as 3D-porous graphene, as these ratios fall within the range of 0.3–0.6 previously reported [51, 52]. Additionally, the O-LIG and HO-LIG undergo a second lasing step, which reduces or removes flakes in the LIG structure. This process potentially results in a less layered structure, further contributing to the observed differences in 2D peaks. On the other hand, regardless of the single or double lasing used to fabricate these LIG materials, the I_D/I_G ratios for the three materials were not significantly different ($p = 0.1443$).

Sensitivity

The ion sensing response of the three distinct LIG-based SC-ISEs, each functionalized with a potassium ISM, was evaluated sequentially by adding KCl while monitoring the electromotive force (EMF) in the electrochemical cell (Fig. 10). For comparison, three potassium-ISEs based on three distinct LIG materials, with superhydrophilic (SI), hydrophobic (O), and highly hydrophobic (SO) characteristics were used. Regression analysis was performed to determine the linear sensing range and the functional correspondence between the ion activity and the EMF. All potassium-ISEs presented significant linear models. The resulting calibration curves, showing a linear detection range spanning from 10^{-5} to 10^{-1} M, are presented in Fig. 10. All fitted models presented statistical significance ($p_{model} < 0.05$) with non-significant lack-of-fit ($p_{LOF} > 0.05$), and the parameters associated with the regression analysis are presented in Table 1. A thorough evaluation of the fitted models is crucial to obtain reliable calibration curves that can accurately make predictions about the ion concentration in unknown samples.

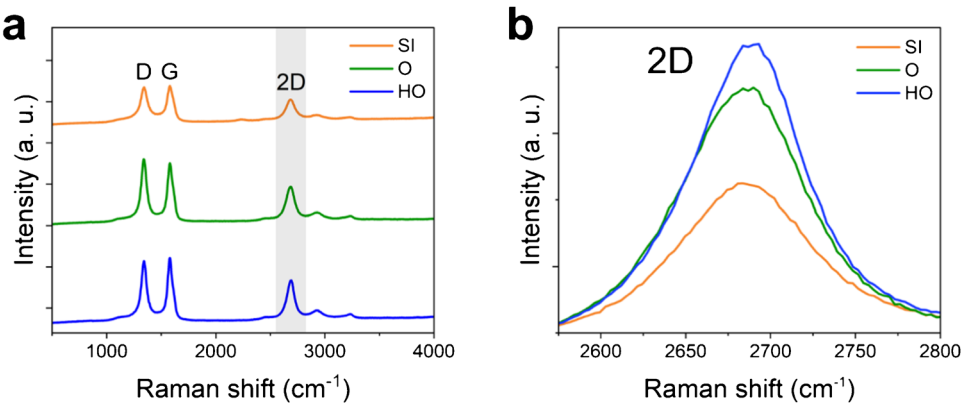

Fig. 9 **a** Raman spectra of the three LIG materials, obtained from ten random points on each sample. **b** Highlighted 2D peaks from the three materials, showing sharper peaks for O-LIG and HO-LIG

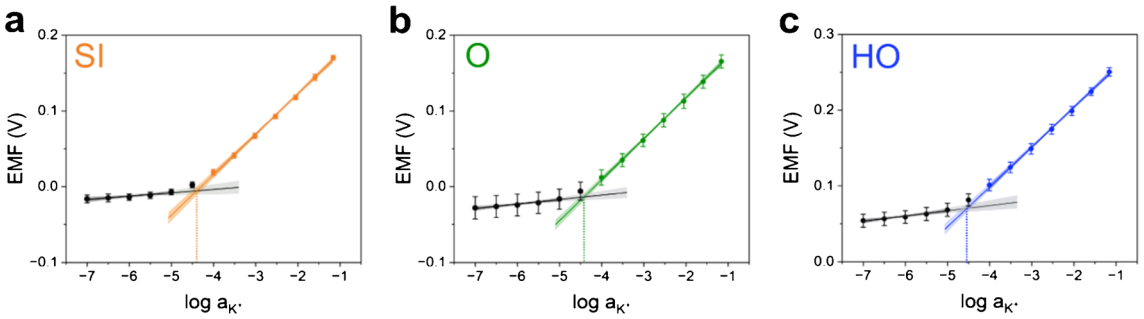

Fig. 10 Plots **a**, **b**, and **c** show the calibration curves ($n=4$) with half-log step additions ranging from 10^{-7} to 10^{-1} M of KCl for the three distinct LIG-based materials. Note: The steps to calculate the potassium ion activity (x-axis) are detailed in the supplementary information

Table 1 Potentiometric potassium responses of three different LIG materials and results of the regression analysis for calibration curves

	Sensitivity (mV/dec)[1]	LOD (ppm)[1,2]	E°' (mV)	$R^2_{adj.}$[3]	p_{Model}[4]	p_{LOF}[5]
SI-LIG	53.2 ± 0.4a	1.515 ± 0.106a	228.8 ± 3.2	0.9947	0.001	0.127
O-LIG	53.8 ± 0.4a	1.429 ± 0.418a	224.8 ± 8.2	0.9758	0.001	0.940
HO-LIG	52.3 ± 1.2a	1.096 ± 0.037a	308.3 ± 4.7	0.9858	0.001	0.812

[1]Mean values ± standard deviation ($n=4$) followed by the same lowercase letter within the same column are non-significantly different ($p>0.05$) according to ANOVA and Tukey's HSD. [2]95% confidence interval (CI) for: SI-LIG (95% CI: 1.2319, 1.7978); O-LIG (95% CI: 1.146, 1.712); OH-LIG (95% CI: 0.8131, 1.3789). [3]R^2_{adj}: adjusted coefficient of determination. [4]p_{Model}: p-value for the adjusted linear model. [5]p_{LOF}: p-value for the model lack-of-fit

All three ISEs exhibited similar sensitivity and LOD values, which were not statistically different at a significance level of 5% ($p=0.056$ and $p=0.093$, respectively). The sub-Nernstian response, characterized by slopes less than 59.2 mV/decade for all three LIG-based ISEs, is likely attributed to small molecule diffusion across the ISM or incomplete conditioning [15]. A result very similar to the obtained sensitivity was achieved with potassium LIG-based ISEs [53], while closer to the theoretical Nernstian values have been reported using alternative materials such as CIM [18] and 3D ordered microporous carbon (3DOM) [54]. Moreover, focusing solely on sensitivity and LOD is insufficient, as it overlooks factors crucial for assessing the long-term reliability of sensors during continuous measurements, such as potential drift and ΔE°'. Even though acceptable calibration curves and LODs are demonstrated, these metrics alone cannot guarantee sustained sensor reliability over extended use. It is important to note that LIG-based electrodes offer a more scalable manufacturing option through direct writing with a laser for carbon-based electrodes, eliminating the need for laborious techniques like ink formulation, application, or chemical or physical vapor deposition growth.

Reproducibility

The reproducibility of the potassium SC-ISE was evaluated by measuring the standard deviation of E°' for the three distinct LIG solid-contact surfaces. Four identical potassium ISEs from the same batch were evaluated for reproducibility, totaling twelve sensors calibrated to compute the ΔE°', according to commonly used protocols [12]. The linear portion of the calibration curves and the corresponding ΔE°' values for each LIG surface are shown in Fig. 11. In this case, SI-LIG showed improved reproducibility (ΔE°'), followed by HO-LIG and O-LIG. In this comparison, it is important to assume that the slopes are not significantly different for the same material, so we are solely comparing the intercepts. As noted by He et al. (2017) [32], more information can be obtained from the batch-to-batch reproducibility of E°' and is recommended. As recently reviewed by Rousseau and Bühlmann (2021) [12], the current state-of-the-art reproducibility values (ΔE°') for capacitive transducers (i.e., solid-contact surfaces with large surface areas such as porous carbon materials and nanostructured noble metals) ranges from 0.7 to 9.2 mV. There are very few examples of low ΔE°' (~ 1.0 mV) with purely capacitive interfaces, with the most reliable ones able to achieve ΔE°' of ± 1.0 mV or lower by using a redox buffer to obtain stability of the interfacial potential [12]. The three LIG surfaces reported here are within this range and in the same order of magnitude as other carbon materials without redox couple addition [12]. These results represent a substantial improvement compared to Chen et al. (2022) for LIG-based potassium ISE [35]. As noted by Lindner and Gyurcsányi (2000), if the change in EMF is slow for long-term measurements

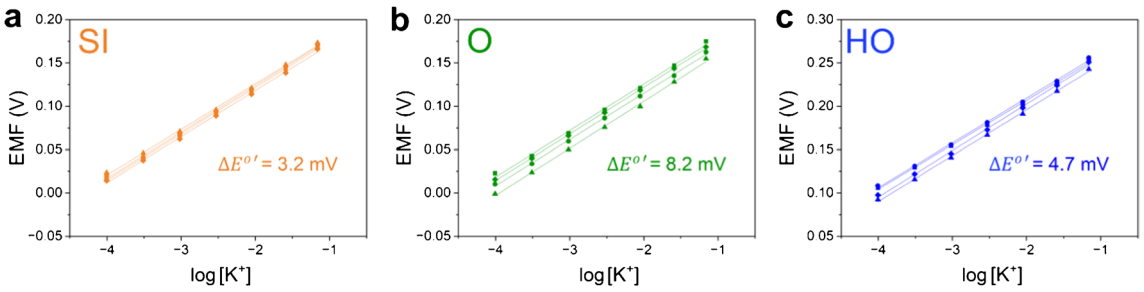

Fig. 11 Plots **a**, **b**, and **c** depict the linear portion of the calibration curves ($n=4$), showing the comparison of reproducibility based on the calculated ΔE°' for the potassium ISEs fabricated on three distinct LIG surfaces (SI-LIG, O-LIG, and HO-LIG). The superhydrophilic and highly hydrophobic surfaces demonstrated the lowest ΔE°' values, indicating superior reproducibility

and the ISE is recalibrated often, the ISE can be used in several practical applications [15].

Furthermore, upon comparing the plots in Fig. 11, the superhydrophilic and highly hydrophobic transducing materials yield the most reproducible ISEs with reduced ΔE°' values. Simply analyzing these plots in isolation, disregarding other parameters, may lead to a different choice for the most proficient ISE compared to the previous discussion, reinforcing the importance of taking a comprehensive view of the situation. As emphasized by previous reviews [12, 15], we recommend always reporting the ΔE°' values and the response slope with the standard deviation to provide comparative metrics to other studies.

Potential stability

Nanostructured carbon materials with high specific surface areas have been extensively used as solid-contact materials, given their high double-layer capacitance due to their large surface areas and highly accessible mesopores [10, 18]. This large surface area attribute can be observed in Fig. 7 for the three different LIG materials with very porous structures. Transducers with a high double-layer capacitance assist with reducing potential drifts over time that initiate from small currents flowing through the potentiometric cell [18]. Since the capacitance of the ion-to-electron transducer layers assists with lowering the EMF drift of the SC-ISE, reporting this value helps interpret the overall performance. The established chronopotentiometry protocol, introduced by Bobacka in 1999 [25], also termed the short-term stability test, is frequently chosen over other methodologies, such as CV and EIS, due to its more straightforward data treatment approach [12]. In this study, chronoamperometry was performed at a constant current of + 0.1 nA and then a current of -0.1 nA for 60 s each, in 0.1 M KCl in water and 0.1 M KPF_6 in acetonitrile as electrolyte solutions (aqueous and non-aqueous solutions) to effectively wet the different LIG surfaces that range from superhydrophilic to highly hydrophobic. Apart from an immediate voltage drop after the current switch, the chronopotentiograms in both electrolyte solutions appear asymmetrical regarding the charging and discharging (Fig. 12), indicating a contribution from redox activity to the electrode capacitance. The calculated low-frequency capacitances (C_L) are presented in Table 2. In both aqueous and non-aqueous systems, the three materials showed no significant differences in capacitance values, with p-values of 0.431 for the materials tested in 0.1 M

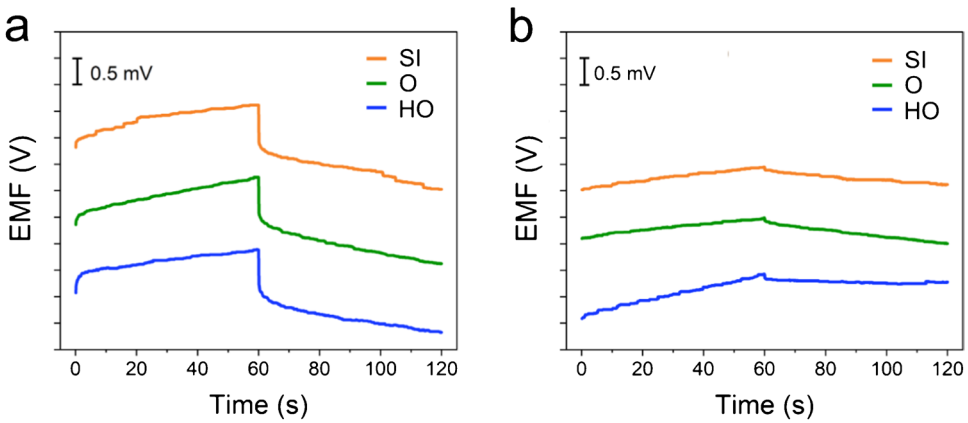

Fig. 12 Chronopotentiometry responses obtained for potassium ISEs utilizing SI-LIG, O-LIG, and HO-LIG materials. The electrodes were tested in two solutions: **a** aqueous solution containing 0.1 M KCl, and **b** acetonitrile solution containing 0.1 M KPF_6 to determine the low-frequency capacitance. A current of ± 1 nA, with anodic current applied first, was applied for 60 s in each experiment

Table 2 Low-frequency capacitances calculated for the three LIG materials in two different media

	C_L in aqueous media (μF)	C_L in non-aqueous media (μF)
SI-LIG	50 ± 4 a	163 ± 7 A
O-LIG	48 ± 3 a	153 ± 15 A
HO-LIG	51 ± 2 a	114 ± 12 A

Mean value ± standard deviation ($n = 3$). For each response variable, values followed by the same lowercase or uppercase letter within the same column are not significantly different ($p < 0.05$) according to ANOVA and Tukey's HSD. Values followed by different lowercase or uppercase letters within the same row are significantly different.

KCl in DI water and 0.700 for those tested in 0.1 M KPF_6 in acetonitrile.

The C_L values are similar to previously published studies with graphene-based potassium-ISEs [55–57]; however, these capacitance values are much lower than other carbon-based solid contacts [26, 30, 58], as reviewed in detail by Chipangura et al. (2023) [10]. Such results further demonstrate that surface wettability, while it plays a substantial role in reducing potential drift and, in turn, increasing the capacitance of nanostructured carbon with high surface areas [10, 12, 23], is not the sole determinant factor. The oxygen content of the three LIG surfaces likely affected both the capacitance and short-term potential drift due to redox activity, in addition to influencing the double capacitance. Moreover, alongside the presence of redox-active groups, edge defects in the carbon structure, which are commonly found in LIG surfaces [14, 35, 40], may contribute to decreased potential stability [59]. On the other hand, the presence of oxygen and edge defects is favorable for other electrochemical methods (e.g., amperometry, coulometry), catalysis, and charge–discharge (e.g., supercapacitor) applications that require a high electrical conductivity.

For potentiometric measurements with SC-ISEs, improvements in electrical conductivity are not essential for ion-to-electron transducers, as little to no (ideally) current should flow during the measurements [10]. Instead, oxygen content should be reduced to limit redox-active groups, preserve hydrophobicity, and suppress water layer formation [54]. Thermal reduction in hydrogen has been applied to minimize the oxygen content of nanostructured carbon (e.g., graphene oxide) [60, 61]. Another strategy involves integrating additional materials onto the solid contact surface. This approach aims to improve ion-to-electron transduction by imparting redox activity to the solid contact [12, 23]. As a result, a thermodynamically stable phase boundary potential is achieved by exchanging electrons between the solid-contact material and the electron conductor and ions with the ISM. These materials include redox self-assembled monolayers, molecular redox buffers, inorganic redox buffers, and conducting polymers, reviewed in detail by Rousseau and Bühlmann (2021) [12].

***Note*:** When evaluating nanostructured carbon materials as solid contacts for ISEs, it is important to measure the capacitance of the actual SC-ISE rather than the bare electrode when using CV and EIS measurements. Additionally, for chronopotentiometry, minimal changes should be expected with or without the ISM, as emphasized by Chipangura et al. (2023)[10] and detailed by Zdrachek and Bakker (2021) [26]. The bulk resistance of ISM greatly impacts capacitance [10, 26]. Indeed, Keresten et al. (2023) [62] showed that this resistance correlates with water uptake and solution ionic strength.

Solutions with the same concentration of potassium-based salts in water and acetonitrile should exhibit different ionic strengths due to differences in solubility and ionization behavior of the salts in the two solvents. However, despite capacitance and dielectric constant (ε) being directly proportional, suggesting that the aqueous medium with $\varepsilon = 80.1$ should exhibit a higher capacitance than acetonitrile with $\varepsilon = 37.2$, the nature of ions in the solution and the membrane play more significant roles [26]. Additionally, solvents with lower viscosity, such as acetonitrile compared to water, facilitate ion mobility, while higher polarity and dielectric constant assist with ion solvation [63]. Consequently, this results in a substantial difference in capacitance values and potential drift between the two electrolyte solutions.

The formation of a water layer between the solid contact and ISM contributes to potential drift and, consequently, is detrimental to calibration-free and long-term continuous measurements. The water layer test proposed by Fibbioli et al. (2000) [28] indicates the presence of an aqueous layer by a positive EMF drift when switching from the primary cation solution to an interfering cation solution, and a negative EMF drift when switching back to the primary cation solution for long equilibration times (Fig. 4b). For this study, the three distinct LIG-ISEs were conditioned for 24 h in 10 mM KCl, followed by measuring the EMF for 4 h. Then, the solution was changed to 10 mM NaCl for 4 h and switched back to the conditioning solution while monitoring the EMF for 16 h, as observed in Fig. 13a (see Table S2 in SI for drift values). Similarly, Fig. 13b shows the resulting EMF responses over 72 h for the three LIG-ISEs (SI-LIG, O-LIG, and HO-LIG) in 10 mM KCl, with substantial differences among the three materials, particularly for SI-LIG, which required a longer time for EMF readings to stabilize. Further, the observed EMF drift significantly decreased ($p = 0.001$) with increasing hydrophobicity, as observed in Table 3, resulting in enhanced potential stability over prolonged periods. As previously highlighted, for monovalent ions, a 1 mV drift accounts for an error of approximately ± 4% in the EMF. The highly hydrophobic

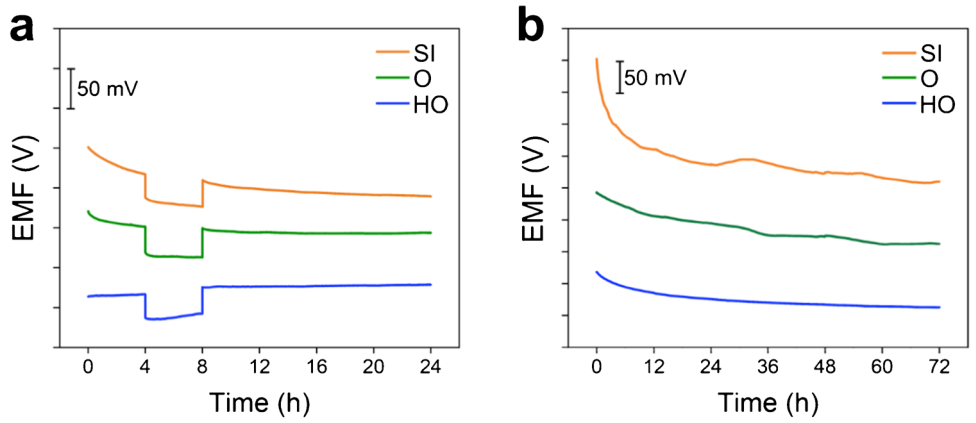

Fig. 13 **a** Water layer test results for potassium ISEs performed for the three different LIG materials (SI-LIG, O-LIG, and HO-LIG), Each ISE was immersed in 0.1 M KCl solution 24 h prior to measurement. At $t = 4$ h, the 0.1 M KCl solution was exchanged for 0.1 M NaCl solution, and at $t = 8$ h, was exchanged for 0.1 M KCl solution. **b** Long-term stability test over a 72-h period in 0.1 M KCl solution, demonstrating an improvement in potential stability with the increase in hydrophobicity of LIG surfaces

Table 3 Long-term (72 h) potential drift estimated for the three LIG materials

	Potential drift (mV/h)
SI-LIG	2.07 ± 0.85 c
O-LIG	1.09 ± 0.18 b
HO-LIG	0.63 ± 0.13 a

Mean values ± standard deviation ($n = 3$) followed by different letters within the same column are significantly different ($p < 0.05$) according to ANOVA and Tukey's HSD.

and hydrophobic properties of doubled-lased LIG, with and without ambient storage, suggest a reduced tendency to form a water layer. This characteristic leads to smaller drifts than previously reported solid contact materials for potassium ISEs, making them promise for long-term continuous applications [64, 65]. The significant reduction in potential drift with increasing hydrophobicity surface is supported by previous works using nanostructured carbon, indicating that hydrophobic materials effectively prevent the formation of a water layer [16, 66–68]. In this regard, efforts to reduce oxygen groups from solid-contact surfaces, aimed at minimizing redox activity while maintaining or enhancing hydrophobicity, have been demonstrated. Functionalization with fluorinated groups on CIM has shown promising results, with minimal to no water layer formation observed during sensing [18]. Remarkably, this approach exhibited a minimal drift of only 1.3 µV/h over 70 h for potassium-ISEs. Similarly, adding a fluorinated acrylic copolymer to carbon black enhanced its hydrophobic nature, helped to hinder the water layer formation, and exhibited an exceptional long-term potential stability of < 1 µV/h over 50 h for a potassium-ISE [30].

All these approaches involve additional steps, which increase the complexity of electrode fabrication. While LIG-based electrodes may not attain the same levels of long-term stability as previously reported [18, 30], laser scribing fabrication offers a more scalable manufacturing option through direct laser writing. This technique enables tuning electrode surface wettability, a feature proven beneficial in numerous applications [14, 35, 40, 53]. Removing oxygen groups from the LIG surface can be done to enhance or maintain hydrophobicity post-fabrication or during the laser induction process [47]. In addition, thermal reduction in hydrogen or inert gas[18, 47, 69], as well as stronger ISM adhesion to the LIG via covalent binding [70, 71] could further improve stability and performance of LIG-ISEs for long-term measurements, including low-frequency capacitance, ΔE°', sensitivity, among others. Future studies should prioritize investigation in these areas.

Conclusions

Since their discovery over 60 years ago, the advantages of SC-ISEs have been demonstrated in multiple applications, with substantial progress being made in understanding and improving the performance of SC-ISEs for ion sensing. In this work, we applied recommended methods to properly characterize and compare SC-ISEs for long-term use as they advance toward calibration-free sensors. While quick response, sensitivity (Nernstian response), and reproducibility (E°' variation) are important for single-use sensors, reduced potential drift is essential for long-term monitoring. In view of the latter, short-term drift via chronopotentiometry experiments is an attractive method to quantify the potential stability of SC-ISEs since they provide a rapid

and straightforward data treatment approach. However, long-term drift measurements are highly recommended, considering chronopotentiometry results can be biased by redox reactions. These include the water layer test and long-term monitoring of the EMF over extended periods (multiple days to weeks). For solid-contact materials that rely on capacitive transduction mechanisms, it is helpful to report the SC-ISE capacitance to understand the overall performance. Methods include chronopotentiometry, EIS, and CV. Although reproducibility (E°' variation) is relevant as a performance metric (intra- and/or inter-batch variations) to single-use and long-term continuous-use sensors and for calibration-free applications, it is not reported as often, which limits comparison among studies. Long-term drift is even more challenging to compare among studies due to the lack of consistency in test parameters and data reporting. Variations include test duration, electrolyte solutions used during the test, type of exposure (e.g., continuous or intermittent), and reporting changes in sensitivity, LOD, and selectivity instead of EMF drift over time. We recommend researchers to consider the criteria presented herein for analyzing and reporting performance characteristics of SC-ISEs to facilitate comparison among different SC-ISEs and advance the field.

Also, in this study, the surface and electrochemical properties of potassium ISEs with three distinct LIG materials (SI-LIG, O-LIG, and HO-LIG) as solid contacts were evaluated to understand their performance using the recommended methods. In particular, the highly hydrophobic and hydrophobic properties of LIG fabricated by a double-lasing process, with and without ambient storage, demonstrated to hinder the formation of a water layer with reduced EMF drift compared to superhydrophilic LIG. SEM and XPS analyses and surface wettability measurements showed that the meso- and micro- porous structures of all three LIG materials contributed to their surface wettability properties and created a large contact area between the solid-contact material and ISM. The large surface area along with the low-frequency capacitances of the SC-ISEs observed via chronopotentiometry contributed to the long-term stability. However, the surface chemistry of the three LIG materials cannot be overlooked. The SI-LIG and HO-LIG showed higher concentrations of oxygen groups than the O-LIG, resulting in redox activity, which is detrimental to potential stability. Even though water layer formation and potential drift have been reduced by hydrophobicity tunning, these are unlikely to be completely eliminated by surface wettability patterning alone. Additionally, the single-lasing process displayed not only superhydrophilic but also superolephilic characteristics, which cannot be explained by the surface oxygen content. Thus, detailed characterization of surface energies should be the focus of future studies to further elucidate the LIG wetting properties. Overall, the hydrophobic and highly hydrophobic LIG surfaces presented comparable results to previous nanostructured carbon potassium ISEs, with the double-lasing process offering a rapid and scalable method to fabricate solid contact materials for ion sensing. To further improve LIG-based ISEs for long-term use, future studies should focus on the removal of oxygen groups during or post-fabrication, and stronger adhesion of ISM to solid contact material.

Supplementary Information The online version contains supplementary material available at https://doi.org/10.1007/s00604-024-06672-y.

Acknowledgements We gratefully acknowledge funding support from the National Science Foundation under award numbers PFI-2141198, CMMI-2037026, and EEC-2231632, the National Institute of Food and Agriculture, U.S. Department of Agriculture, award number 2020-67021-31375, 2021-67021-34457, 2023-38821-39796, and 2018-67016-27578, awarded as a Center of Excellence.

Funding This research was funded by the National Science Foundation and by the National Institute of Food and Agriculture, US Department of Agriculture. The award numbers are listed in the Acknowledgements.

Data availability The data that support the findings of this study are available from the corresponding authors, upon reasonable request.

Declarations

Ethical approval This research did not involve human or animal samples.

Competing interests J. C. Claussen is a senior associate editor of *Microchimica Acta* and was not involved in the peer-review process of this manuscript. The remaining authors declare no competing interests.

References

1. Bakker E, Bühlmann P, Pretsch E (1999) Polymer membrane ion-selective electrodes-what are the limits? Vol. 11, Electroanalysis. Wiley-VCH Verlag; 915–33.
2. Bard AJ, Faulkner LR (2001) Electrochemical methods: fundamentals and applications, 2nd edn. Wiley, New York, 833 p
3. McNaught AD, Wilkinson A (1997) Compendium of chemical terminology, 2nd edn. Blackwell Science, Oxford, 464 p
4. Buck RP, Lindner E (1994) Recomendations for nomenclature of ion-selective electrodes (IUPAC recommendations 1994). Pure Appl Chem 66(12):2527–2536
5. Hernández R, Riu J, Rius FX (2010) Determination of calcium ion in sap using carbon nanotube-based ion-selective electrodes. Analyst 135(8):1979–1985
6. Bakker E, Pretsch E (2005) Potentiometric sensors for trace-level analysis. TrAC - Trends in Anal Chem 24(3 SPEC. ISS):199–207
7. Criscuolo F, Hanitra MIN, Taurino I, Carrara S, De Micheli G (2021) All-Solid-State Ion-Selective Electrodes: A Tutorial for Correct Practice. IEEE Sens J 21(20):22143–22154
8. Dillingham PW, Alsaedi BSO, Granados-Focil S, Radu A, McGraw CM (2020) Establishing Meaningful Limits of Detection for Ion-Selective Electrodes and Other Nonlinear Sensors. ACS Sens 5(1):250–257
9. Chen LD, Mandal D, Pozzi G, Gladysz JA, Bühlmann P (2011) Potentiometric sensors based on fluorous membranes doped

with highly selective ionophores for carbonate. J Am Chem Soc 133(51):20869–20877
10. Chipangura YE, Spindler BD, Bühlmann P, Stein A (2023) Design criteria for nanostructured carbon materials as solid contacts for ion-selective sensors. Adv Mater 36(8):2309778
11. Steed JW, Gale PA (2012) Supramolecular chemistry: from molecules to nanomaterials, 1st edn. Wiley, New York, 4014 p
12. Rousseau CR, Bühlmann P (2021) Calibration-free potentiometric sensing with solid-contact ion-selective electrodes. TrAC - Trends in Anal Chem 140:116277. https://doi.org/10.1016/j.trac.2021.116277
13. Bakker E (1996) Determination of Improved Selectivity Coefficients of Polymer Membrane Ion-Selective Electrodes by Conditioning with a Discriminated Ion. J Electrochem Soc 143(4):83–85
14. Hjort RG, Soares RRA, Li J, Jing D, Hartfiel D, Chen B, Van Belle B, Soupir M, Smith E, McLamore E, Claussen JC, Gomes CL (2022) Hydrophobic laser-induced graphene potentiometric ion-selective electrodes for nitrate sensing. Microchim Acta 189(3):122
15. Lindner E, Gyurcsányi RE (2009) Quality control criteria for solid-contact, solvent polymeric membrane ion-selective electrodes. J Solid State Electrochem 13(1):51–68
16. Hu J, Stein A, Bühlmann P (2016) Rational design of all-solid-state ion-selective electrodes and reference electrodes. TrAC - Trends in Anal Chem 76:102–114
17. Cheong YH, Ge L, Lisak G (2021) Highly reproducible solid contact ion selective electrodes: emerging opportunities for potentiometry – a review. Anal Chim Acta 1162:338304
18. Hu J, Zou XU, Stein A, Bühlmann P (2014) Ion-selective electrodes with colloid-imprinted mesoporous carbon as solid contact. Anal Chem 86(14):7111–7118
19. Bratov A, Abramova N, Ipatov A (2010) Recent trends in potentiometric sensor arrays – a review. Anal Chim Acta 678(2):149–159
20. Parrilla M, Cuartero M, Padrell Sánchez S, Rajabi M, Roxhed N, Niklaus F et al (2019) Wearable all-solid-state potentiometric microneedle patch for intradermal potassium detection. Anal Chem 91(2):1578–1586
21. Parrilla M, Cuartero M, Crespo GA (2019) Wearable potentiometric ion sensors. TrAC - Trends in Anal Chem 110:303–20. https://doi.org/10.1016/j.trac.2018.11.024
22. Cuartero M, Pankratova N, Cherubini T, Crespo GA, Massa F, Confalonieri F et al (2017) In situ detection of species relevant to the carbon cycle in seawater with submersible potentiometric probes. Environ Sci Technol Lett 4(10):410–415
23. Shao Y, Ying Y, Ping J (2020) Recent advances in solid-contact ion-selective electrodes: Functional materials, transduction mechanisms, and development trends. Chem Soc Rev 49(13):4405–4465
24. Das Suprem R, Nian Q, Cargill AA, Hondred JA, Ding S, Saei M et al (2016) 3D nanostructured inkjet printed graphene: Via UV-pulsed laser irradiation enables paper-based electronics and electrochemical devices. Nanoscale 8(35):15870–9
25. Bobacka J (1999) Potential stability of all-solid-state ion-selective electrodes using conducting polymers as ion-to-electron transducers. Anal Chem 71(21):4932–4937
26. Zdrachek E, Bakker E (2021) Ion-to-electron capacitance of single-walled carbon nanotube layers before and after ion-selective membrane deposition. Microchim Acta 188(5):21–23
27. Zhao Q, Wajert JC, Anderson JL (2010) Polymeric ionic liquids as CO2 selective sorbent coatings for solid-phase microextraction. Anal Chem 82(2):707–713
28. Fibbioli M, Morf WE, Badertscher M, De Rooij NF, Pretsch E (2000) Potential drifts of solid-contacted ion-selective electrodes due to zero-current ion fluxes through the sensor membrane. Electroanalysis 12(16):1286–1292
29. Li X, Forouzandeh F, Kakanat AJ, Feng F, Banham DWH, Ye S et al (2018) Surface characteristics of microporous and mesoporous carbons functionalized with pentafluorophenyl groups. ACS Appl Mater Interfaces 10(2):2130–2142
30. Paczosa-Bator B (2015) Ion-selective electrodes with superhydrophobic polymer/carbon nanocomposites as solid contact. Carbon N Y 11(95):879–887
31. Amemiya S, Bühlmann P, Pretsch E, Rusterholz B, Umezawa Y (2000) Cationic or anionic sites? Selectivity optimization of ion-selective electrodes based on charged ionophores. Anal Chem 72(7):1618–1631
32. He N, Papp S, Lindfors T, Höfler L, Latonen RM, Gyurcsányi RE (2017) Pre-polarized hydrophobic conducting polymer solid-contact ion-selective electrodes with improved potential reproducibility. Anal Chem 89(4):2598–2605
33. Law KY (2014) Definitions for hydrophilicity, hydrophobicity, and superhydrophobicity: getting the basics right. J Phys Chem Lett 5(4):686–688
34. Lamour G, Hamraoui A, Buvailo A, Xing Y, Keuleyan S, Prakash V et al (2010) Contact angle measurements using a simplified experimental setup. J Chem Educ 87(12):1403–1407
35. Chen B, Johnson ZT, Sanborn D, Hjort RG, Garland NT, Soares RRA et al (2022) Tuning the structure, conductivity, and wettability of laser-induced graphene for multiplexed open micro fluidic environmental biosensing and energy storage devices. ACS Nano 16:15–28
36. Wenzel RN (1936) Resistance of solid surfaces to wetting by water. Ind Eng Chem. 28(8):988–94. Available from: https://pubs.acs.org/sharingguidelines
37. B D Cassie A, Baxter S (1934) Wettability of porous surfaces. Transactions of the Faraday Society. 40:546–51
38. Dębosz M, Kozma J, Porada R, Wieczorek M, Paluch J, Gyurcsányi RE et al (2021) 3D-printed manifold integrating solid contact ion-selective electrodes for multiplexed ion concentration measurements in urine. Talanta 1:232
39. Zdziennicka A, Krawczyk J, Szymczyk K, Jańczuk B (2017) Components and parameters of liquids and some polymers surface tension at different temperature. Colloids Surf A Physicochem Eng Asp 20(529):864–875
40. Soares RRA, Hjort RG, Pola CC, Jing D, Cecon VS, Claussen JC et al (2023) Ion-selective electrodes based on laser-induced graphene as an alternative method for nitrite monitoring. Microchimica Acta 190(1):43. https://doi.org/10.1007/s00604-022-05615-9
41. Li Z, Wang Y, Kozbial A, Shenoy G, Zhou F, McGinley R et al (2013) Effect of airborne contaminants on the wettability of supported graphene and graphite. Nat Mater 12(10):925–931
42. Hurst JM, Kim MA, Peng Z, Li L, Liu H (2019) Assessing and mitigating surface contamination of carbon electrode materials. Chem Mater 31(18):7133–7142
43. Behrent A, Borggraefe V, Baeumner AJ (2024) Laser-induced graphene trending in biosensors: understanding electrode shelf-life of this highly porous material. Anal Bioanal Chem 416(9):2097–2106
44. Chen X, Farber M, Gao Y, Kulaots I, Suuberg EM, Hurt RH (2003) Mechanisms of surfactant adsorption on non-polar, air-oxidized and ozone-treated carbon surfaces. Carbon N Y 41(8):1489–1500
45. Nasser J, Lin J, Zhang L, Sodano HA (2020) Laser induced graphene printing of spatially controlled super-hydrophobic/hydrophilic surfaces. Carbon N Y 1(162):570–578
46. Bai S, Tang Y, Lin L, Ruan L, Song R, Chen H et al (2022) Investigation of micro/nano formation mechanism of porous graphene induced by CO2 laser processing on polyimide film. J Manuf Process 1(84):555–564
47. Li Y, Luong DX, Zhang J, Tarkunde YR, Kittrell C, Sargunaraj F et al (2017) Laser-Induced Graphene in Controlled Atmospheres:

From Superhydrophilic to Superhydrophobic Surfaces. Adv Mater 29(27):1–8
48. Dallinger A, Steinwender F, Gritzner M, Greco F (2023) Different roles of surface chemistry and roughness of laser-induced graphene: implications for tunable wettability. ACS Appl Nano Mater 6(18):16201–16211
49. Rathinam K, Singh SP, Li Y, Kasher R, Tour JM, Arnusch CJ (2017) Polyimide derived laser-induced graphene as adsorbent for cationic and anionic dyes. Carbon N Y 124(2):515–24. https://doi.org/10.1016/j.carbon.2017.08.079
50. Lin J, Peng Z, Liu Y, Ruiz-Zepeda F, Ye R, Samuel ELG et al (2014) Laser-induced porous graphene films from commercial polymers. Nat Commun 5:1–8. https://doi.org/10.1038/ncomms6714
51. Muzyka K, Xu G (2022) Laser-induced graphene in facts, numbers, and notes in view of electroanalytical applications: a review. Electroanalysis 34(4):574–589
52. Soares RRA, Hjort RG, Pola CC, Jing D, Cecon VS, Claussen JC, Gomes CL (2023) Ion-selective electrodes based on laser-induced graphene as an alternative method for nitrite monitoring. Microchim Acta 190(1):43
53. Kucherenko IS, Sanborn D, Chen B, Garland N, Serhan M, Forzani E et al (2020) Ion-selective sensors based on laser-induced graphene for evaluating human hydration levels using urine samples. Adv Mater Technol 5(6):1–9
54. Lai CZ, Fierke MA, Stein A, Bühlmann P (2007) Ion-selective electrodes with three-dimensionally ordered macroporous carbon as the solid contact. Anal Chem 79(12):4621–4626
55. Liu Y, Liu Y, Meng Z, Qin Y, Jiang D, Xi K et al (2020) Thiol-functionalized reduced graphene oxide as self-assembled ion-to-electron transducer for durable solid-contact ion-selective electrodes. Talanta 1:208
56. Li F, Ye J, Zhou M, Gan S, Zhang Q, Han D et al (2012) All-solid-state potassium-selective electrode using graphene as the solid contact. Analyst 137(3):618–623
57. Ping J, Wang Y, Wu J, Ying Y (2011) Development of an all-solid-state potassium ion-selective electrode using grapheme as the solid-contact transducer. Electrochem commun 13(12):1529–1532
58. Paczosa-Bator B (2012) All-solid-state selective electrodes using carbon black. Talanta 15(93):424–427
59. Miller PR, Xiao X, Brener I, Burckel DB, Narayan R, Polsky R (2014) Microneedle-based transdermal sensor for on-chip potentiometric determination of K+. Adv Healthc Mater 3(6):876–881
60. Wei A, Wang J, Long Q, Liu X, Li X, Dong X et al (2011) Synthesis of high-performance graphene nanosheets by thermal reduction of graphene oxide. Mater Res Bull 46(11):2131–2134
61. Sofer Z, Jankovský O, Šimek P, Soferová L, Sedmidubský D, Pumera M (2014) Highly hydrogenated graphene via active hydrogen reduction of graphene oxide in the aqueous phase at room temperature. Nanoscale 6(4):2153–2160
62. Keresten VM, Bykov AG, Gofman IV, Solovyeva EV, Vlasov AY, Mikhelson KN (2023) Non-constancy of the bulk resistance of ionophore-based ion-selective membranes within the Nernstian response range: A semi-quantitative explanation. J Memb Sci 9(683):121830
63. Wu Z, Zou J, Shabanian S, Golovin K, Liu J (2022) The roles of electrolyte chemistry in hard carbon anode for potassium-ion batteries. Chem Eng J 1:427
64. Fierke MA, Lai CZ, Bühlmann P, Stein A (2010) Effects of architecture and surface chemistry of three-dimensionally ordered macroporous carbon solid contacts on performance of ion-selective electrodes. Anal Chem 82(2):680–688
65. Park HJ, Jeong JM, Yoon JH, Son SG, Kim YK, Kim DH et al (2020) Preparation of ultrathin defect-free graphene sheets from graphite via fluidic delamination for solid-contact ion-to-electron transducers in potentiometric sensors. J Colloid Interface Sci 15(560):817–824
66. Hjort RG, Soares RRA, Li J, Jing D, Hartfiel L, Chen B et al (2022) Hydrophobic laser-induced graphene potentiometric ion-selective electrodes for nitrate sensing. Microchimica Acta 189(122):1–11. https://doi.org/10.1007/s00604-022-05233-5
67. Veder JP, De Marco R, Clarke G, Chester R, Nelson A, Prince K et al (2008) Elimination of undesirable water layers in solid-contact polymeric ion-selective electrodes. Anal Chem 80(17):6731–6740
68. Crespo GA, Macho S, Rius FX (2008) Ion-selective electrodes using carbon nanotubes as ion-to-electron transducers. Anal Chem 80(4):1316–1322
69. Li X, Banham D, Feng F, Forouzandeh F, Ye S, Kwok DY et al (2015) Wettability of colloid-imprinted carbons by contact angle kinetics and water vapor sorption measurements. Carbon N Y 87(C):44–60
70. Choi KR, Chen XV, Hu J, Bühlmann P (2021) Solid-Contact pH sensor with covalent attachment of ionophores and ionic sites to a poly(decyl methacrylate) matrix. Anal Chem 93(50):16899–16905
71. Choi KR, Troudt BK, Bühlmann P (2023) Ion-selective electrodes with sensing membranes covalently attached to both the inert polymer substrate and conductive carbon contact. Angew Chem 62(28):e202304674